

Exciting Pseudospin Dependent Edge States in Plasmonic Metasurfaces

Matthew Proctor,^{*,†,‡} Richard V. Craster,[†] Stefan A. Maier,^{¶,‡} Vincenzo Giannini,[§]
and Paloma A. Huidobro^{||,‡}

[†]*Department of Mathematics, Imperial College London, London, SW7 2AZ, UK*

[‡]*Department of Physics, Imperial College London, London, SW7 2AZ, UK*

[¶]*Chair in Hybrid Nanosystems, Nanoinstitut München, Faculty of Physics,
Ludwig-Maximilians-Universität München, 80539, München, Germany*

[§]*Instituto de Estructura de la Materia (IEM), Consejo Superior de Investigaciones
Científicas (CSIC), Serrano 121, 28006, Madrid, Spain*

^{||}*Instituto de Telecomunicações, Instituto Superior Técnico-University of Lisbon, Avenida
Rovisco Pais 1, 1049-001 Lisboa, Portugal*

E-mail: matthew.proctor12@imperial.ac.uk

Abstract

We study a plasmonic metasurface that supports pseudospin dependent edge states confined at a subwavelength scale, considering full electrodynamic interactions including retardation and radiative effects. The spatial symmetry of the lattice of plasmonic nanoparticles gives rise to edge states with properties reminiscent of the quantum spin Hall effect in topological insulators. However, unlike the spin-momentum locking characteristic of topological insulators, these modes are not purely unidirectional and their propagation properties can be understood by analysing the spin angular momentum of the electromagnetic field, which is inhomogeneous in the plane of the lattice. This spin

determines the propagation direction of the mode under a near-field excitation source.

We also study the optical response under far-field excitation and discuss in detail the effects of radiation and retardation.

Keywords

plasmonics, metasurface, nanoparticle array, topological photonics, nanophotonics, pseudospin

1 Introduction

Topological insulators are materials which are insulating in the bulk but which have conduction surface states protected against disorder.¹ The remarkable properties of these states in electronic systems has inspired the search for photonic topological insulators (PTIs), which aim to guide and manipulate photons with the same level of control and efficiency.^{2–6} Systems which possess these effects whilst preserving time reversal symmetry are appealing as they do not require complicated experimental setups such as strong magnetic fields or bianisotropic coupling. Motivated by this, a proposal to emulate the quantum spin Hall (QSH) effect in photonic crystals was presented by Wu and Hu in Ref. 7. Effects reminiscent of the QSH phase such as a band inversion between dipolar and quadrupolar modes, and pseudospin dependent edge states are realised but, rather than relying on the time reversal symmetric pairs characteristic of electronic systems, they instead rely on the spatial symmetry of the lattice structure. As a result, the edge states have reduction in backscattering over trivial ones.^{8,9} The method has since been applied to a variety of bosonic systems,^{10–14} and has recently experimentally been demonstrated in the visible regime.¹⁵

The combination of topological effects with plasmonics offers the possibility of precisely controlling light on the nanoscale. The strong enhancement and localisation of electric fields due to localised surface plasmon (LSP) resonances¹⁶ is a widely employed platform for

light confinement on the nanoscale.^{17,18} Plasmonic metasurfaces can be formed by arranging plasmonic nanoparticles in two-dimensional (2D) lattices, where the LSPs become delocalised across the whole metasurface as collective resonances. The optical properties of metasurfaces are then determined by the individual nanoparticle elements as well as the geometry of the lattice.^{19,20} The tunable optical properties of metasurfaces makes them versatile tools for the manipulation of light on the nanoscale.^{21,22} For instance, appropriately designed plasmonic metasurfaces can host spin dependent directional states which can couple to valley excitons when interfaced to 2D materials.²³

One-dimensional (1D) chains of dielectric and metallic nanoparticles were some of the first systems used for the investigation of topological phases in nanophotonics,^{24–30} in particular systems analogous to the Su-Schrieffer-Heeger (SSH) model, which hosts topologically protected edge states in 1D. In the plasmonic chain, initial studies into these topological states were limited to the quasistatic approximation (QSA)³¹ despite the well known radiative effects which are of great importance for large enough nanoparticles and retardation which is important at large lattice periods^{32,33} or at very small periods, where higher order multipolar effects occur.³⁴ Indeed, beyond the quasistatic limit, the plasmonic SSH chain becomes non-Hermitian and band structures are distorted compared to the quasistatic model, with effects such as polariton splitting at the light line.³⁵ In addition, the ubiquitous bulk-edge correspondence of topological insulators has been shown to break down due to retardation.³⁶ 2D plasmonic systems, including graphene and arrays of plasmonic nanoparticles have also been considered for hosting topological states. Time reversal broken effects reliant on magnetic fields have been proposed for graphene plasmons.^{37,38} Honeycomb lattices of plasmonic nanoparticles have been investigated in the quasistatic limit, where a direct analogy between the tight binding model in graphene and nearest neighbour approximation in plasmonics can be made.^{39–41} More recently, theoretical and experimental investigations have shown how the long range, retarded interactions affect the physical behaviour of the system.^{42,43} Here, we consider the lattice geometry proposed in Ref. 7, shown in Figure 1, to study pseudospin

dependent edge states in plasmonic metasurfaces. This scheme has been considered in 2D arrays of plasmonic nanoparticles in the QSA.⁴⁴ In this work, we go beyond this approximation and study the realisation of electromagnetic modes resembling the QSH effect on a plasmonic metasurface, including full electrodynamic interactions in our description of the system.

We use semi-analytical techniques to investigate plasmonic metasurfaces. These consist of a triangular lattice with unit cells containing six nanoparticles arranged in a hexagon, Figure 1a. We begin by outlining the coupled dipole method used to model these arrays in section 2. Then we investigate the behaviour of the modes supported by the metasurface in section 3. By calculating the eigenmodes of the infinite lattice, we characterise the band inversion process which occurs between a *shrunk* phase (where nanoparticles in the unit cell are displaced towards the centre) and an *expanded* phase (where they are displaced outwards from the centre). The response of the infinite system is also studied under far-field excitation. In section 4, we then consider the interface between two phases in a semi-infinite ribbon layout to elucidate the nature of the edge states that emerge due to the band inversion between the two phases. We characterise their pseudospin dependence, showing that it is related to the spin angular momentum of the electromagnetic fields, and probe these states in the near-field with a magnetic dipole source. By investigating the effect of the source position, we unambiguously show that, unlike the unidirectional edge states characteristic of topological insulators, the directionality of these edge states depends on the source position. Finally, in section 5, we highlight the radiative and retardation effects on the edge states.

2 Design and set up of the plasmonic metasurface

The metasurface we consider here consists of a 2D array of metal nanorods (modelled as spheroidal nanoparticles) arranged in the lattice shown in Figure 1a. The unit cell contains six nanoparticles of radius r and height h arranged in a hexagon separated by nearest

neighbour spacing R with lattice vectors \mathbf{a}_1 and \mathbf{a}_2 , as shown in the figure. In the regime $R > 3r$, the nanoparticles can be considered as point dipoles and higher order resonances can be neglected.^{32,45} A nanoparticle at position \mathbf{r}_i with polarisability $\alpha(\omega)$ supports a dipole moment \mathbf{p}_i when excited by an external field \mathbf{E}_i . For a lattice of nanoparticles, a coupled dipole equation can be written which describes the dipole moment of a nanoparticle induced by an external field plus the sum of all neighbouring dipole moments,

$$\frac{1}{\alpha(\omega)}\mathbf{p}_i = \mathbf{E}_i + \sum_{i \neq j} \hat{\mathbf{G}}(\mathbf{r}_i - \mathbf{r}_j, \omega) \mathbf{p}_j, \quad (1)$$

where the dyadic Green's function $\hat{\mathbf{G}}$, describes the interactions between point dipoles, and is given by,

$$\hat{\mathbf{G}}(\mathbf{r}_i - \mathbf{r}_j, \omega) = k^2 \frac{e^{ikr}}{r} \left[\left(1 + \frac{i}{kr} - \frac{1}{k^2 r^2} \right) \hat{\mathbf{I}} - \left(1 + \frac{3i}{kr} - \frac{3}{k^2 r^2} \right) \mathbf{n} \otimes \mathbf{n} \right]. \quad (2)$$

Here, $k = \sqrt{\epsilon_B} \omega / c$ is the wavenumber of the surrounding medium, with $\sqrt{\epsilon_B}$ the permittivity of the surrounding environment (which is assumed to be the vacuum throughout this work, $\epsilon_B = 1$), and $r = |\mathbf{r}_i - \mathbf{r}_j|$ is the distance between nanoparticles, with $\mathbf{n} = (\mathbf{r}_i - \mathbf{r}_j) / |\mathbf{r}_i - \mathbf{r}_j|$ the unit vector in the direction along the line that joins two nanoparticles.

In equation 1, the polarisability, $\alpha(\omega)$, describes the optical response of an individual nanoparticle. The static polarisability for a spheroidal nanoparticle is written,

$$\alpha_s(\omega) = \frac{V}{4\pi} \frac{\epsilon(\omega) - 1}{1 + L(\epsilon(\omega) - 1)}, \quad (3)$$

where $\epsilon(\omega)$ is the dielectric function of the metal, V is the spheroid volume, and L is the static geometrical factor which is dependent on the radius and height of the nanoparticle; for a sphere $L = \frac{1}{3}$.⁴⁶ The dielectric function of the nanoparticles is given by the Drude model,

$$\epsilon(\omega) = \epsilon_\infty - \frac{\omega_p^2}{\omega^2 + i\omega\gamma}. \quad (4)$$

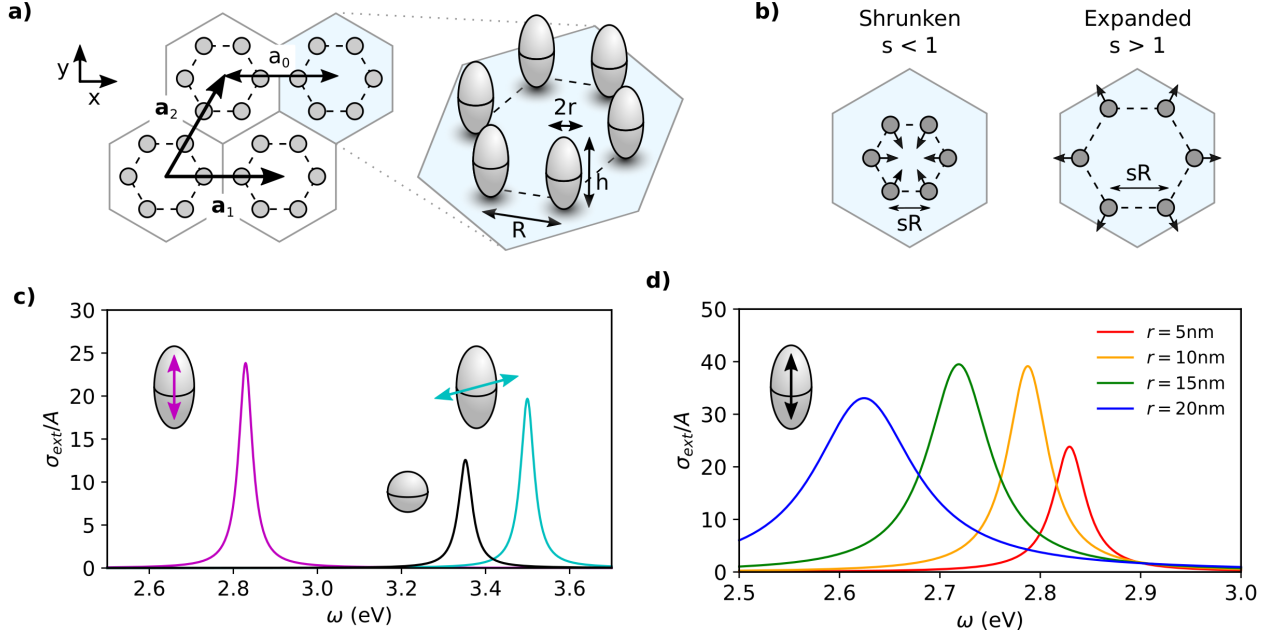


Figure 1: Metal rods are arranged on a plane to form a plasmonic metasurface, and their optical response is modelled including radiative and retarded effects. a) Layout of the lattice of plasmonic nanoparticles, including a close up of the arrangement of particles in the unit cell, b) The perturbation of the unit cell into shrunken and expanded phases with scaling parameter s . $s = 1$ corresponds to the unperturbed honeycomb lattice. c) Extinction cross sections σ_{ext} , normalized to geometrical cross section, of silver spheroidal nanoparticles showing the splitting of in-plane (blue) and out-of-plane (pink) resonances, d) σ_{ext} of nanoparticles with increasing radius, showing the radiative broadening and redshifting of the plasmon resonance.

Throughout the work we consider silver nanoparticles, with $\epsilon_\infty = 5$, $\omega_p = 8.9\text{eV}$ and $\gamma = 2\pi\tau = 17\text{fs}$.⁴⁷ The static polarisability neglects radiative effects which are essential for describing larger nanoparticles. We take this into account by means of the modified long wavelength approximation (MLWA),

$$\alpha_{\text{MLWA}}(\omega) = \frac{\alpha_s(\omega)}{1 - \frac{k^2}{l_E} D \alpha_s(\omega) - i \frac{2k^3}{3} \alpha_s(\omega)}, \quad (5)$$

where l_E is the spheroid major axis half length and D is a dynamic geometrical factor; $D = 1$ for a sphere.⁴⁶ The importance of the radiative correction for spheroidal silver nanoparticles is exemplified in Figure 1c. The extinction cross section σ_{ext} for a spheroidal nanoparticle with radius $r = 5\text{nm}$ and height $h = 20\text{nm}$, as well as a spherical nanoparticle with radius $r = 5\text{nm}$ is shown. We normalise to the cross sectional area A perpendicular to the dipole moment. The nanoparticle supports two resonance modes: one where the dipole is aligned with the minor axis (in-plane) and one with the major axis (out-of-plane). The out-of-plane resonance becomes redshifted and well separated in frequency from the in-plane resonance, which allows us to investigate the out-of-plane and in-plane modes separately. The increased radiative effect on a single nanoparticle is demonstrated by the extinction cross section for larger radii, up to $r = 20\text{nm}$, where the resonance becomes broader and continues to be redshifted, Figure 1d. Whilst the static polarisability adequately describes the behaviour of the smallest nanoparticle sizes, the MLWA incorporates the effects of dynamic depolarisation and the radiative correction and is necessary to correctly model particles of radius above $\sim 10\text{ nm}$.

3 Spectral response of the metasurface

We start by considering the optical response of the plasmonic metasurface in the expanded and shrunken phases, Figure 1b. We do so by setting up an infinite lattice of nanoparticles

and applying periodic boundary conditions to Equation 1 by writing the external electric field and dipole moments as periodic Bloch functions. An eigenvalue equation can then be written,

$$\left(\frac{1}{\alpha(\omega)} - \hat{\mathbf{H}}(\mathbf{q}, \omega)\right) \cdot \mathbf{p} = \mathbf{E}, \quad (6)$$

where the Hamiltonian $\hat{\mathbf{H}}(\mathbf{q}, \omega)$ has elements,

$$H_{ij} = \begin{cases} \sum_{\mathbf{R}} \hat{\mathbf{G}}(\mathbf{r}_i - \mathbf{r}_j + \mathbf{R}, \omega) e^{i\mathbf{q} \cdot \mathbf{R}} & i \neq j \\ \sum_{|\mathbf{R}| \neq 0} \hat{\mathbf{G}}(\mathbf{R}, \omega) e^{i\mathbf{q} \cdot \mathbf{R}} & i = j \end{cases}, \quad (7)$$

with \mathbf{q} , the Bloch wavevector. We note that the Hamiltonian is a 6×6 matrix since we restrict our study to the out-of-plane modes, such that there is one single degree of freedom for each particle in the unit cell. The in-plane modes of a honeycomb lattice of plasmonic nanoparticles have been studied elsewhere⁴¹ and being well shifted in frequencies, they are completely decoupled to the out-of-plane modes. Finally, we note that sums in the Hamiltonian are conditionally convergent due to the slowly decaying $1/r$ term and so additional manipulation is required to converge these expressions (see Methods).

Figure 2 shows the spectral response of the plasmonic metasurface under study. We consider nanoparticles with radius $r = 5\text{nm}$ and height $h = 20\text{nm}$, nearest neighbour spacing $R = 20\text{nm}$ and lattice constant $a_0 = 60\text{nm}$. To calculate the eigenvalues and eigenvectors of the periodic lattice we solve Equation 6 without an incident field. Initially, in order to keep the eigenvalue problem linear we take the QSA and only consider the quickly decaying $1/r^3$ term in the Green's function. However, we choose to go beyond the nearest neighbour approximation and include interactions between all particles in the lattice.⁴⁸ The band structure of a metasurface with the nanoparticles arranged in a honeycomb lattice is shown in Figure 2a. Instead of using the conventional rhombic unit cell, we take the larger hexag-

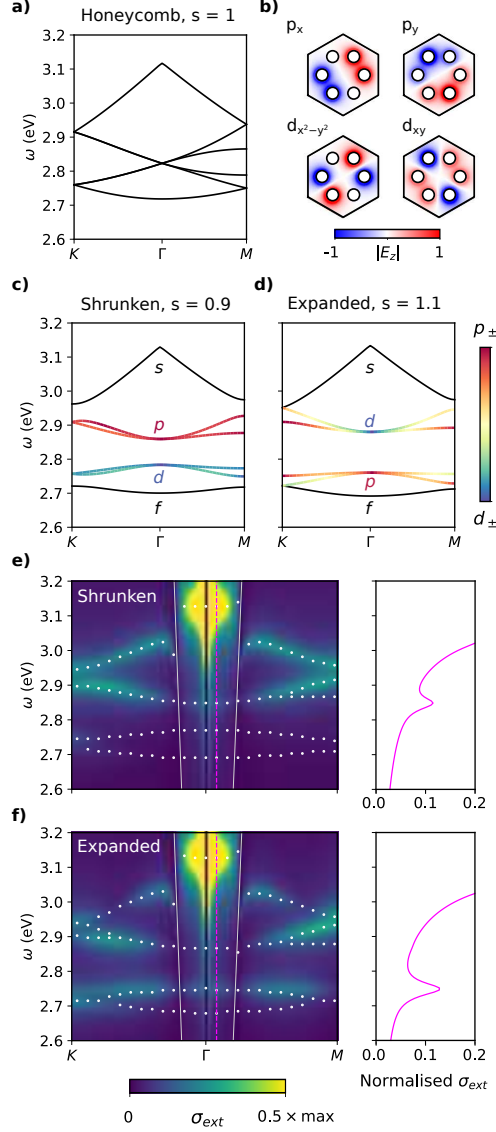


Figure 2: Exciting plasmonic metasurfaces from the far-field. Nanoparticles have radius $r = 5\text{nm}$ and height $h = 20\text{nm}$, and the lattice constant $a_0 = 60\text{nm}$. a) Bulk dispersion relations of the out-of-plane modes of the honeycomb plasmonic lattice, including all neighbours in the quasistatic approximation (QSA), b) Electric fields of the quadrupolar and dipolar modes (at lower and higher energies, respectively) of an isolated hexagon of nanoparticles, including full GF interactions. c) Dispersion relations for the shrunken ($s = 0.9$) and d) expanded ($s = 1.1$) systems. The bands are coloured according to their dipolar (p) or quadrupolar (d) nature, showing the band inversion at Γ between shrunken and expanded phases. The monopolar (s) and hexapolar (f) bands are not involved in the inversion. e), f) Extinction cross sections, normalised to the maximum, under excitation with an external field including full retarded Green's function (GF) interactions and radiative polarisabilities for the shrunken and expanded phases. The dots highlight all the modes in the system, some of which are dark in an external field. The light line is shown with a thin white line. σ_{ext} at a fixed wavevector (purple dotted line) is shown in the right hand plots.

onal cell such that the Brillouin zone (BZ) of the honeycomb lattice becomes folded and the Dirac points at K and K' are mapped onto each other to create a doubly degenerate point at Γ as shown in the figure.⁷ Whereas the original honeycomb lattice is formed of two triangular sublattices, the system is now formed of six sublattices corresponding to the six nanoparticles in the unit cell. In the QSA, assuming nearest neighbour interactions, the Dirac points of the honeycomb plasmonic lattice occur at the surface plasmon resonance frequency w_{sp} ⁴¹ and the band structure is symmetrical about this frequency.⁴⁴ This is no longer the case due to the sublattice symmetry breaking interaction term between particles of the same sublattice in neighbouring unit cells. Figure 2c shows the band structures for metasurfaces with shrunken (left) and expanded (right) unit cells. The bands are labelled as s , p , d , f , indicating monopolar, dipolar, quadrupolar and hexapolar characters. This was determined by calculating the overlap with the eigenstates of an isolated hexagon of nanoparticles, with the dipole and quadrupole shown in Figure 2b. In both the shrunken and expanded phases, we see how the ordering of the modes is opposite to that obtained in photonic crystals and other bosonic analogues, with the monopolar mode being the highest in energy and the hexapolar being the lowest one,^{7,13,14,49} and we fully justify these results later. Next, we notice that near the centre of the BZ, there is a mode inversion between the shrunken and expanded phases. This is evident from the colour scale, which encodes the dipolar/quadrupolar character of the modes. In the shrunken phase ($s < 1$), the band above the band gap is dipolar and the one below is quadrupolar (Figure 2c). On the other hand, for the expanded phase ($s > 1$) they become inverted at Γ (Figure 2d). The degeneracy of the bands above and below the gap at Γ for the shrunken and expanded lattices suggests linear combinations of these modes can be taken, $p_{\pm} = (p_x \pm ip_y)$ and $d_{\pm} = (d_{x^2-y^2} \pm id_{xy})$, which correspond to pseudospins; taking positive or negative combinations gives clockwise or anticlockwise rotations.

After characterising the eigenstates in the QSA, we now consider the full electrodynamic interaction between the nanoparticles by including all terms in the Green's function, and

explore retardation and radiative effects by calculating the extinction cross section of the system when excited by an external field. We show the response of the system in the shrunken and expanded phase over the BZ in Figure 2e-f (contour plots). The incident plane wave is defined as $\mathbf{E} = (E_x, E_y, E_z)$, where the field components satisfy Maxwell's equations and $k_0^2 = q_{\parallel}^2 + q_z^2$. Above the light line, the wave is propagating in the z direction, where $q_z = i\sqrt{q_{\parallel}^2 - k_0^2}$ and below the light line it is evanescent, $q_z = \sqrt{k_0^2 - q_{\parallel}^2}$, which allows us to probe the eigenstates in this region of the spectrum. Starting at Γ , the incident field has no z -component meaning out-of-plane dipoles cannot be excited. As soon as we move away from Γ , we begin to excite out-of-plane polarised modes. The highest energy mode corresponds to a monopolar mode, with all dipole moments in the unit cell pointing in the same direction. For neighbouring nanoparticles with dipole moments which are in phase, the displacement of charge on the first nanoparticle will cause a force opposite to the displacement of charge on the second nanoparticle, which increases the restoring force and resonant frequency of the mode.⁴⁸ In a dimer, for example, this corresponds to the bonding mode lying at a higher energy compared to the anti-bonding mode. Although this hybridisation of modes in plasmonic nanoparticles may seem unexpected, it has been demonstrated experimentally.⁵⁰ In the infinite lattice, the bonding nature of the monopolar mode across the whole system causes it to be highly radiant and so dominates the response of the lattice for propagating waves. Nevertheless, we are still able to examine the peaks in extinction cross section at lower frequencies. By symmetry arguments, only the dipolar mode is excitable by a plane wave for small wavevectors, \mathbf{q} . The extinction cross section of the system agrees with the characterisation of the modes in the QSA. In the shrunken phase, the higher energy dipolar mode is visible in the extinction cross section whereas in the expanded phase a band inversion occurs. This inversion between dipolar and quadrupolar modes close to the BZ centre constitutes a signature to distinguish both metasurface phases, since it can be detected experimentally by far-field measurements.⁴⁹ In the right panels of Figure 2e-f we show the extinction spectrum at a fixed incident momentum, \mathbf{q} : the resonance peak

corresponding to the dipolar mode is visible for the shrunken structure at higher energies than for the expanded structure. In Figure 2e-f, we plot the loci of peaks in the spectral function based on the effective polarisability (see Methods), to make all of the modes visible, even those which are dark in an external field. These peaks qualitatively agree with the QSA dispersion relation with only a slight redshift due to the radiative correction given that all the length scales in the system are very subwavelength. Retardation effects are most apparent in the highest energy band at the light line, where polariton splitting occurs, but this does not affect the band inversion at Γ . Finally, the lowest energy band is a hexapolar mode where all dipole moments are in anti-phase meaning such a mode cannot be excited by a plane wave, and it is not visible in the extinction cross section for most of the BZ.

4 Pseudospin edge states in finite systems

After characterising the modes in the metasurface, we now look at the edge states between regions of different phases. As discussed earlier, the band inversion between different phases is reminiscent of the QSH effect and thus pseudospin dependent, directional edge states are anticipated. In order to study the edge states, we consider an interface between the two different phases of the metasurface. In the calculations, a finite ribbon of a region in the expanded phase is cladded with regions in the shrunken phase so that we have a finite structure along the direction \mathbf{a}_2 , and we apply Bloch periodicity along \mathbf{a}_1 . Figure 3a shows the band structure of the ribbon, calculated with retardation (black lines), and also in the QSA (grey lines). In the case of full electrodynamics interactions, the Green's function was linearised by letting $\omega = \omega_{sp}$ and the static polarisability was assumed (see Methods). Two edge states can be seen clearly within the band gap (we colour the retarded solution, as we will explain below). Importantly, the edge states do not join the bulk modes, rather they reconnect with each other at the edges of the BZ. This is a fundamental distinction with topological edge states since it means it is possible, by a continuous change of parameters,

to remove these states from the band gap; which indicates that these edge states are not resistant to backscattering.⁵¹ In Figure 3b, we also plot the spectral function of the system with radiative corrections in the polarisability, which accounts for the frequency shift (in this plot we let the Drude losses $\gamma = 0.01\text{eV}$ to improve the visibility of the edge states). Similarly to the bulk dipolar and quadrupolar bands, we see the edge states do not interact strongly with the light line although the radiative broadening and redshift is apparent. Since the pseudospin effect is reliant on the C_{6v} symmetry of the bulk system which is necessarily broken at the interface between the shrunken and expanded region there will always be a ‘minigap’ between the edge states at Γ which will never fully close. The amount of perturbation between shrunken and expanded phase determines the size of the bulk band gap and as well as the size of the minigap. To minimise the gap, the perturbation along the edge can be graded; the edge states are then excitable across the whole band gap.^{11,44}

To investigate the pseudospin nature of the modes we now look at the two eigenstates of the expanded/shrunken interface with opposite group velocity, and at a frequency ω in the upper band. These are shown as points s_1 and s_2 in Figure 3a. We first plot the time averaged Poynting vector $\mathbf{S} = \frac{1}{2}\text{Re}(\mathbf{E} \times \mathbf{H}^*)$ along with the out-of-plane electric field E_z in Figure 3c, demonstrating that the edge modes are confined to the interface between the two regions. The Poynting vector (arrows) characterises the flow of electromagnetic energy, which is in opposite directions for wavevectors with opposite sign. However, it is important to note that in inhomogeneous, dispersive media it can be argued that the Poynting vector does not necessarily accurately characterise a spin or pseudospin.^{52,53} More appropriately, we also consider the spin angular momentum in the plane of the lattice, which is given by, $T = \text{Im}(\mathbf{H}^* \times \mathbf{H})$. We plot this quantity over the same region as the Poynting vector in Figure 3c, where its inhomogeneous character across the lattice is evident, with varying magnitude and sign across the interface. To determine the pseudospin dependence of the edge states, we integrate the spin angular momentum T over a region shown in red in Figure 3d, for wavevectors q_{\parallel} across the whole BZ, and we plot the edge states with this colour code in

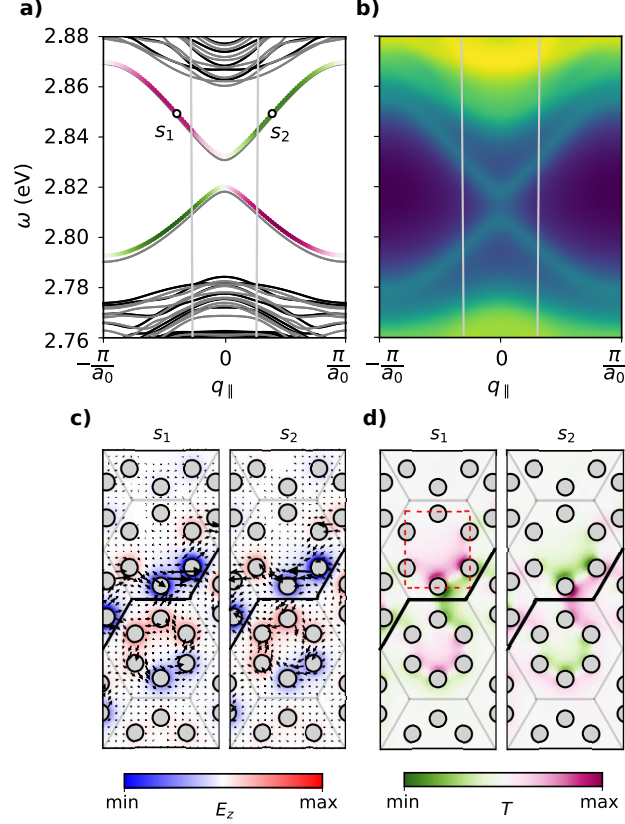


Figure 3: Pseudospin modes along the interface between metasurfaces in expanded and shrunken phases. a) Dispersion relations of a semi-infinite ribbon with a 28 unit cell region in the expanded phase ($s = 1.1$) cladded with two 6 unit cell regions in the shrunken phase ($s = 0.9$). Results obtained in the QSA including all neighbours are shown in grey and results including full GF interactions are shown in black, with both in the non-radiative regime. We highlight the edge modes in this case with colours according to their pseudospin, characterised by spin angular momentum T . b) Spectral function of the retarded, radiative system with Drude losses $\gamma = 0.01\text{eV}$. The frequency shift in the edge states compared to the QSA in a) is due to the radiative effects, c) Spin angular momentum T for modes s_1 and s_2 , marked in a). T is integrated in the red region colour the edge states in a), d) out-of-plane electric field E_z for s_1 and s_2 . The arrows show the time averaged Poynting vector \mathbf{S} , demonstrating the directionality of the edge states.

the dispersion relation in panel a. At the edges of the BZ there is maximum mixing between pseudospins meaning $T = 0$, but as we move towards the centre we see either edge state acquires an opposite pseudospin. This pattern of opposite pseudospins travelling in opposite directions is akin to the QSH effect. Again, we note that since in this system the two edge modes are linked through a pseudo-time reversal operator,⁷ which is only rigourously defined at Γ , there is not complete protection against backscattering.

We now consider the excitation of edge modes with a localised source, and its relation to the spin angular momentum. In Figure 3c we showed, for s_1 , the spin angular momentum T is positive within the hexagon of nanoparticles immediately above and below the edge, and the sign switches for s_2 . This is in agreement with the switching of the directionality given by the Poynting vector. However, outside of these regions the sign of T is opposite. Importantly, this means that the spin angular momentum of the mode is actually position dependent, and that it does not agree with the proposed pseudospin for the modes. This position dependence has implications on the excitation of unidirectional modes which we show by modelling a finite array of nanoparticles with an interface between an expanded and shrunken region. To fully understand how the propagation along the edge is dependent on the source and its position, we consider an interface with zero material losses; the edge state is prevented from reflecting off the hard boundary with the vacuum by slowly increasing material losses at these boundaries. We place a right circularly polarised magnetic dipole source with magnetic field $\mathbf{H} = H_x + iH_y$ at the various positions shown in Figure 3a. We choose the excitation frequency from Figure 3b as $\omega = 2.83\text{eV}$. The emission of the magnetic dipole source placed in the plasmonic lattice will be modified due to the surrounding environment. This is characterised by the Purcell factor P_F , the ratio of emitted power of a magnetic dipole to the emitted power in free space P_M ,⁵⁴

$$P_M = \frac{\mu_0}{4\pi} \frac{\omega^4 |\mathbf{m}|^2}{3c^3}, \quad (8)$$

where μ_0 is the vacuum permeability and \mathbf{m} is the magnetic dipole moment. The Purcell factor as a function of source position is shown in Figure 4b (dotted orange line). The enhancement is greatest when the source is close to the metallic nanoparticles in the lattice, but we note it is generally modest due to the distance between the source and nanoparticles.

To characterise the directionality of the energy flow along the edge, we integrate the Poynting vector through a plane perpendicular to the interface and metasurface, and we plot this as solid lines in Figure 4b; with purple and green corresponding to flow to the right (P_R) and left (P_L), respectively. Regions in which the coupled dipole approximation does not hold are shaded. Starting at \mathbf{r}_1 , the flow of energy is predominantly to the right as expected from the right hand polarisation of the source, which couples to the right-propagating pseudospin mode. Importantly there is still a fraction of energy travelling to the left which demonstrates the existence of pseudospin mixing. As the source is moved towards \mathbf{r}_2 the flow is completely to the right before quickly flipping to the opposite direction. From \mathbf{r}_2 to \mathbf{r}_3 the energy flow again changes sign as the source moves from an area with negative spin angular momentum to an area with positive spin angular momentum. The emission pattern can then be predicted by the spin angular momentum in real space in Figure 3c, rather than by the pseudospin character of the mode. We emphasise that we have used a right hand polarised source throughout, which suggests one should always expect energy flow in the right direction. In Figure 4c-d we show the stark difference in directionality along the edge depending on the position of the source (magenta star). We consider the same right-circularly polarized source placed at two different positions. In Figure 4c we choose the optimal placement for excitation in the expected direction, and in Figure 4d the least optimal placement. All bosonic systems possessing these lattice symmetries, such as the photonic crystal, will also possess these position dependent directional modes when excited with a circularly polarised source.⁵⁵ In the left and right panels, we show the electric field intensity, $|\mathbf{E}|^2$, at plane cut perpendicular to the metasurface in the left and right directions. We note that the edge state is not only confined to the edge in the plane of the metasurface but also out of the

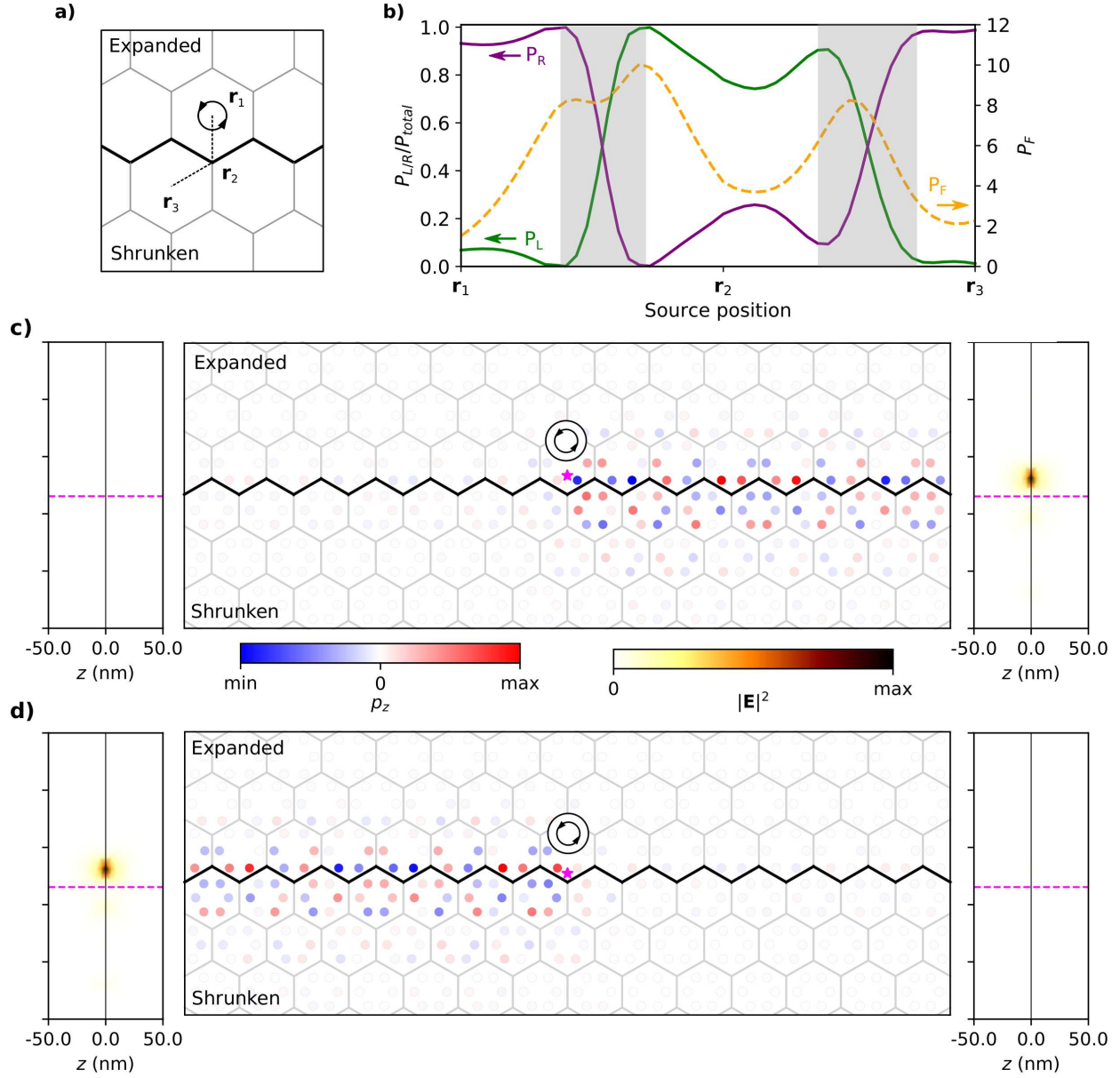


Figure 4: Exciting pseudospin edge states with near-field probes. a) A right circularly polarised magnetic dipole is placed at positions along the path shown to excite the edge state between expanded and shrunken regions in the metasurface, b) The fraction of power travelling left and right, $P_{L/R}$, as well as the Purcell factor P_F are dependent on source position across the edge. Although the source is right circularly polarised, it will excite an edge state in the opposite direction for some positions along the edge. (Regions where the coupled dipole approximation does not hold are shaded), c) Pseudospin edge state excited by a source at the optimal position for a right travelling mode. The middle panel shows the dipole moments in the plane of the metasurface (xy plane). The left and right panels show the electric field intensity $|\mathbf{E}|^2$ perpendicular to the metasurface (yz plane), showing the mode is strongly confined in the out-of-plane direction z , d) A source with the same polarisation as in c) is placed at the least optimal position showing excitation in the opposite direction.

plane at subwavelength scales.

5 Retardation and Radiative Effects

We finally discuss in detail the effect of retardation and radiation in the pseudospin edge states. While so far we have considered a very subwavelength period and nanoparticle size, we have already seen the effect of retarded interactions which cause the band structure to be altered with respect to the QSA, in particular close to the light line, and the radiative broadening and redshifting of resonances. Radiative effects become more apparent for larger nanoparticles, with very large broadenings and shifts as in the single particle extinction cross section shown in Figure 1d; effects which are not captured in the QSA. On the other hand, it is important to note that retardation can have striking consequences not only on bulk band structures but also on the properties of edge states. It has been shown for example how in the 1D plasmonic SSH model, retardation can result in the breakdown of bulk boundary correspondence and the disappearance of edge states.³⁶ To investigate the effects of retardation in the 2D system studied here, we excite an interface between expanded and shrunken regions in a ribbon with a plane wave at a finite wavevector above the light line, $q = 0.15\pi/a_0$, and calculate the extinction cross section for increasing lattice constants a_0 .

In Figure 5a, we show the extinction cross section for a metasurface with an interface between the two phases for silver nanoparticles with radius 5nm and height 20nm. We let the Drude losses $\gamma = 0.01\text{eV}$ as in Figure 5b and highlight the edge states with white dots for visibility. As in the infinite lattice, in the quasistatic and nearest neighbour approximations, the edge states are expected to be symmetrical about the plasma frequency ω_{sp} (dotted purple line). In contrast, when radiative effects are taken into account, there are substantial shifts in the edge state frequencies. Initially, for $a_0 = 60\text{nm}$ the edge states are well separated from the bulk but as the lattice constant increases up to 90nm the bulk modes close up and

the edge states are lost. We calculate the full width at half maximum (FWHM) of the highest energy edge state at $a_0 = 60\text{nm}$ where $\text{FWHM} = 0.0059\text{eV}$. As an aside, this edge state has a larger cross section as along the interface the nanoparticles form a bonding-like state (Figure 5c, top) whereas the lower energy edge state has an anti-bonding distribution which leads to lower cross section (Figure 5c, bottom). In Figure 5b we show the cross section for nanoparticles with radius 10nm and height 40nm , with lattice constant varying from 120 to 180nm . Here, the edge states become significantly redshifted far below ω_{sp} . Again we measure the FWHM, at $a_0 = 120\text{nm}$, $\text{FWHM} = 0.0077\text{eV}$ demonstrating the broadening of the mode for larger nanoparticles. We note that these widths are smaller than the Drude losses since the lattice structure modifies the optical response by increasing the quality factor.^{17,18}

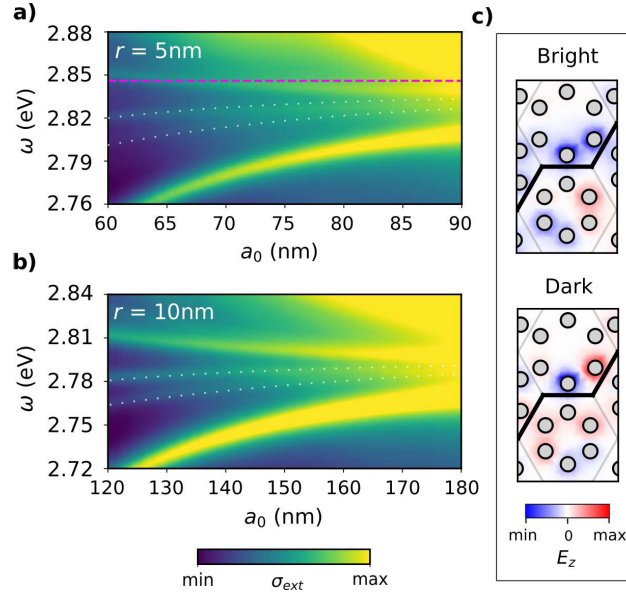


Figure 5: far-field excitation of pseudospin edge states showing radiative and retardation effects. Extinction cross section for ribbon system under plane wave excitation at $q_x = 0.15\pi/a$ for increasing lattice constants a_0 with Drude losses $\gamma = 0.01\text{eV}$. a) For particle radius $r = 5\text{nm}$ and height $h = 20\text{nm}$. The surface plasmon frequency ω_{sp} is shown as the purple dotted line, b) For particle radius $r = 10\text{nm}$ and height $h = 40\text{nm}$. The bands are shifted to lower frequencies, far below ω_{sp} , c) out-of-plane electric field patterns in a cut across the metasurface for the upper and lower energy edge states for the parameters in a). The upper mode is bright as it has a bonding symmetry along the edge allowing it to be excited by a plane wave, while the lower mode is dark.

6 Conclusion

In this work we have presented a study of spin dependent edge states in a plasmonic metasurface. These states rely on lattice symmetries and are similar to the quantum spin Hall effect in topological insulators. By going beyond the quasistatic approximation and including retardation and radiative effects, we model the plasmonic system appropriately and show how the long range interactions result in a more complex band structure than the QSA. The bands involved in the band inversion are not greatly affected by retardation, and they provide a signature for far-field measurements. We note that the ordering in energy of the modes of the plasmonic metasurface are opposite to what is seen in photonic crystals,⁷ with the dipolar modes lying at higher energies than the quadrupolar modes for the non-inverted bands.

Importantly, we determine the spin angular momentum of the edge modes, and show that this is the quantity that characterises the directionality of the modes. Remarkably, this leads to a more complex behaviour which can be opposite to what would be expected from a direct analogy with the QSH effect. We emphasise that these conclusions are valid not only for the plasmonic metasurface but for any bosonic system with this lattice.⁵⁵ We probe the spin angular momentum by looking at the excitation of the edge states in the near-field by a magnetic dipole source. By varying the position of the source, we highlight how the location is essential in exciting a purely unidirectional state. In agreement with the spin angular momentum characterisation of the edge in the ribbon we show that in some positions a source will excite a mode in completely the opposite way to the expected direction.

Finally, we have also considered the optical response of the plasmonic metasurface and the edge modes under far-field excitation, showing the effect of radiative and retardation effects for the larger radius nanoparticles and larger lattice constants. Although the edge states persist for larger nanoparticles, we observe a radiative broadening and shift in frequency which is naturally not captured in a quasistatic approximation. For increasing lattice constants, the bulk modes close up and eventually the edge states are indistinguishable, which provides

a parameter regime for which these edge states could be experimentally observed.

7 Methods

7.1 Lattice sums

The summations in the Hamiltonian in Equation 7 are conditionally convergent. Firstly, we will consider sums including the origin term and split these into long range and short/medium range terms,

$$S_{\text{incl}} = \sum_{\mathbf{R}} e^{i\mathbf{q}\cdot\mathbf{R}} \hat{\mathbf{G}}(\mathbf{r}, \omega) = S_L + S_{SM} \quad (9)$$

where $S_L = k^2 \sum_{\mathbf{R}} e^{i\mathbf{q}\cdot\mathbf{R}} e^{ikr} \frac{1}{r}$ and $S_{SM} = k^2 \sum_{\mathbf{R}} e^{i\mathbf{q}\cdot\mathbf{R}} e^{ikr} \left(\frac{ik}{r^2} - \frac{1}{r^3} \right)$. The slowly converging S_L term is handled by using Ewald's method.⁵⁶ This splits the real space sum into two and then takes the Fourier transform of one part using Poisson's summation, resulting in a sum over the reciprocal lattice. The sum is optimised with a Ewald parameter to ensure the real space and reciprocal space sum converge within approximately the same number of lattice constants. The S_{SM} term converges rapidly above the light line when $k_0 < |\mathbf{q}|$. Outside of this region the first few terms within a radius R_{min} are added and then the rest of the sum is calculated numerically by approximating the summation as an integral,⁴⁸

$$S_{SM} \approx k^2 \sum_{\mathbf{R}=0}^{\mathbf{R}_{min}} e^{i\mathbf{q}\cdot\mathbf{R}} e^{ikr} \left(\frac{ik}{r^2} - \frac{1}{r^3} \right) + k^2 \int_{R_{min}}^{\infty} e^{i\mathbf{q}\cdot\mathbf{R}} e^{ikr} \left(\frac{ik}{r^2} - \frac{1}{r^3} \right) \quad (10)$$

For sums excluding the origin,

$$S_{\text{excl}} = \sum_{\mathbf{R} \neq 0} e^{i\mathbf{q}\cdot\mathbf{R}} \hat{\mathbf{G}}(\mathbf{R}, \omega) \quad (11)$$

the integral method from Ref. 48 is used. For ribbons which are infinite in only one direction, the summations converge easier and so no techniques are used to speed up convergence.⁴¹

In the quasistatic approximation, we only consider the short range $1/r^3$ term which converges quickly when including all neighbours, in both the infinite lattice and semi-infinite ribbon. We note that this method of including all neighbours results in a kink at Γ in one of the modes of the infinite lattice which is due to the group velocity necessarily being zero at the centre of the BZ.⁴⁸

7.2 Linearised Green's Function

In Figure 3, we linearise the Green's function to investigate the spin angular momentum semi-analytically. For the retarded Green's function and radiative polarisabilities the eigenvalue problem is non-linear and non-Hermitian,

$$\left(\hat{\mathbf{H}}(\mathbf{q}, \omega) - \frac{1}{\alpha(\omega)} \hat{\mathbf{I}} \right) \cdot \mathbf{p} = 0 \quad (12)$$

To avoid the computational complexity of searching for complex ω solutions we linearise the Green's function by making the approximation $\omega = \omega_{sp}$, the surface plasmon frequency. This is valid for the size of nanoparticles considered here since ω varies faster in the polarisability term than in the Green's function. As particle size increases the approximation becomes less valid close to the light line. We then have a Hamiltonian, $\hat{\mathbf{H}}(\mathbf{q}, \omega_{sp})$ for which eigenvalues λ and eigenvectors \mathbf{p} are found at each \mathbf{q} and band structures are calculated by rearranging $\lambda = 1/\alpha(\omega)$ to find ω , for the static polarisability.

7.3 Spectral Function

The spectral function method relies on an effective polarisability formulation of the system.^{41,48} Recall the eigenvalue problem for a non-zero external field,

$$\left(\hat{\mathbf{H}}(\mathbf{q}, \omega) - \frac{1}{\alpha(\omega)} \hat{\mathbf{I}} \right) \cdot \mathbf{p} = \mathbf{M} \cdot \mathbf{p} = \mathbf{E} \quad (13)$$

which we rewrite as $\mathbf{p} = \alpha_{\text{eff}} \mathbf{E}$. The effective polarisability $\alpha_{\text{eff}} = 1/\lambda$ for eigenvalues of \mathbf{M} , λ . The spectral function is analogous to the extinction cross section but rather than describing the system when excited by a well defined external field instead characterises all modes in the system in the retarded, radiative regime, regardless of whether they are bright or dark modes. This corresponds to the forced oscillation of each mode of the lattice at some driving frequency ω and Bloch wavevector \mathbf{q} . The spectral function is defined,

$$\sigma_{\text{spectral}} = \frac{4\pi\omega}{c} \sum_i \text{Im}(\alpha_{\text{eff}}^{(i)}) \quad (14)$$

where the sum is over the number of elements in the unit cell in the infinite lattice or the super cell in the semi-infinite ribbon. Peaks in the spectral function will correspond to the real part of the band structures from the linearised Green's function.

Acknowledgement

We acknowledge fruitful discussions with A. García-Etxarri. M.P., R.V.C. and P.A.H. acknowledge funding from the Leverhulme Trust. P.A.H. also acknowledges funding from Fundação para a Ciência e a Tecnologia and Instituto de Telecomunicações under project CEECIND/03866/2017. S.A.M. and R.V.C. acknowledge funding from EPSRC Programme Grant “Mathematical Fundamentals of Metamaterials” (EP/L024926/1). S.A.M. additionally acknowledges the Lee-Lucas Chair in Physics.

References

- (1) Hasan, M. Z.; Kane, C. L. Colloquium: topological insulators. *Reviews of Modern Physics* **2010**, *82*, 3045.
- (2) Ozawa, T.; Price, H. M.; Amo, A.; Goldman, N.; Hafezi, M.; Lu, L.; Rechtsman, M. C.;

- Schuster, D.; Simon, J.; Zilberberg, O.; Carusotto, I. Topological photonics. *Reviews of Modern Physics* **2019**, *91*, 015006.
- (3) Rider, M. S.; Palmer, S. J.; Pocock, S. R.; Xiao, X.; Arroyo Huidobro, P.; Giannini, V. A perspective on topological nanophotonics: Current status and future challenges. *Journal of Applied Physics* **2019**, *125*, 120901.
- (4) Khanikaev, A. B.; Shvets, G. Two-dimensional topological photonics. *Nature Photonics* **2017**, *11*, 763.
- (5) Lu, L.; Joannopoulos, J. D.; Soljačić, M. Topological photonics. *Nature Photonics* **2014**, *8*, 821.
- (6) Silveirinha, M. G. Proof of the bulk-edge correspondence through a link between topological photonics and fluctuation-electrodynamics. *Physical Review X* **2019**, *9*, 011037.
- (7) Wu, L.-H.; Hu, X. Scheme for achieving a topological photonic crystal by using dielectric material. *Physical Review Letters* **2015**, *114*, 223901.
- (8) Orazbayev, B.; Kaina, N.; Fleury, R. Chiral Waveguides for Robust Waveguiding at the Deep Subwavelength Scale. *Physical Review Applied* **2018**, *10*, 054069.
- (9) Orazbayev, B.; Fleury, R. Quantitative robustness analysis of topological edge modes in C6 and valley-Hall metamaterial waveguides. *Nanophotonics* **2019**, *8*, 1433–1441.
- (10) Jiang, Z.; Gao, Y.-f.; He, L.; Sun, J.-p.; Song, H.; Wang, Q. Manipulation of pseudo-spin guiding and flat bands for topological edge states. *Physical Chemistry Chemical Physics* **2019**, 11367–11375.
- (11) Chaunsali, R.; Chen, C.-W.; Yang, J. Subwavelength and directional control of flexural waves in zone-folding induced topological plates. *Physical Review B* **2018**, *97*, 054307.

- (12) Barik, S.; Miyake, H.; DeGottardi, W.; Waks, E.; Hafezi, M. Two-dimensionally confined topological edge states in photonic crystals. *New Journal of Physics* **2016**, *18*, 113013.
- (13) Yves, S.; Fleury, R.; Berthelot, T.; Fink, M.; Lemoult, F.; Lerosey, G. Crystalline metamaterials for topological properties at subwavelength scales. *Nature Communications* **2017**, *8*, 16023.
- (14) Yves, S.; Fleury, R.; Lemoult, F.; Fink, M.; Lerosey, G. Topological acoustic polaritons: robust sound manipulation at the subwavelength scale. *New Journal of Physics* **2017**, *19*, 075003.
- (15) others,, et al. Probing the Band Structure of Topological Silicon Photonic Lattices in the Visible Spectrum. *Physical Review Letters* **2019**, *122*, 117401.
- (16) Maier, S. A. *Plasmonics: Fundamentals and Applications*; Springer Science & Business Media, 2007.
- (17) Giannini, V.; Fernández-Domínguez, A. I.; Heck, S. C.; Maier, S. A. Plasmonic nanoantennas: fundamentals and their use in controlling the radiative properties of nanoemitters. *Chemical Reviews* **2011**, *111*, 3888–3912.
- (18) Kravets, V.; Kabashin, A.; Barnes, W.; Grigorenko, A. Plasmonic Surface Lattice Resonances: A Review of Properties and Applications. *Chemical Reviews* **2018**, *118*, 5912–5951.
- (19) Meinzer, N.; Barnes, W. L.; Hooper, I. R. Plasmonic meta-atoms and metasurfaces. *Nature Photonics* **2014**, *8*, 889.
- (20) Baur, S.; Sanders, S.; Manjavacas, A. Hybridization of lattice resonances. *ACS Nano* **2018**, *12*, 1618–1629.

- (21) Wang, W.; Ramezani, M.; Väkeväinen, A. I.; Törmä, P.; Rivas, J. G.; Odom, T. W. The rich photonic world of plasmonic nanoparticle arrays. *Materials Today* **2018**, *21*, 303–314.
- (22) Monticone, F.; Alu, A. Metamaterial, plasmonic and nanophotonic devices. *Reports on Progress in Physics* **2017**, *80*, 036401.
- (23) Chervy, T.; Azzini, S.; Lorchat, E.; Wang, S.; Gorodetski, Y.; Hutchison, J. A.; Berciaud, S.; Ebbesen, T. W.; Genet, C. Room temperature chiral coupling of valley excitons with spin-momentum locked surface plasmons. *ACS Photonics* **2018**, *5*, 1281–1287.
- (24) Poddubny, A.; Miroshnichenko, A.; Slobozhanyuk, A.; Kivshar, Y. Topological Majorana states in zigzag chains of plasmonic nanoparticles. *ACS Photonics* **2014**, *1*, 101–105.
- (25) Slobozhanyuk, A. P.; Poddubny, A. N.; Miroshnichenko, A. E.; Belov, P. A.; Kivshar, Y. S. Subwavelength topological edge states in optically resonant dielectric structures. *Physical Review Letters* **2015**, *114*, 123901.
- (26) Downing, C. A.; Weick, G. Topological collective plasmons in bipartite chains of metallic nanoparticles. *Physical Review B* **2017**, *95*, 125426.
- (27) Downing, C. A.; Weick, G. Topological plasmons in dimerized chains of nanoparticles: robustness against long-range quasistatic interactions and retardation effects. *The European Physical Journal B* **2018**, *91*, 253.
- (28) Kruk, S.; Slobozhanyuk, A.; Denkova, D.; Poddubny, A.; Kravchenko, I.; Miroshnichenko, A.; Neshev, D.; Kivshar, Y. Edge states and topological phase transitions in chains of dielectric nanoparticles. *Small* **2017**, *13*, 1603190.
- (29) Kruk, S.; Poddubny, A.; Smirnova, D.; Wang, L.; Slobozhanyuk, A.; Shorokhov, A.;

- Kravchenko, I.; Luther-Davies, B.; Kivshar, Y. Nonlinear light generation in topological nanostructures. *Nature Nanotechnology* **2019**, *14*, 126.
- (30) Wu, R. P.; Zhang, Y.; Lee, K.; Wang, J.; Yu, S.; Fung, K. H. Dynamic long range interaction induced topological edge modes in dispersive gyromagnetic lattices. *Physical Review B* **2019**, *99*, 214433.
- (31) Ling, C.; Xiao, M.; Chan, C.; Yu, S.; Fung, K. H. Topological edge plasmon modes between diatomic chains of plasmonic nanoparticles. *Optics Express* **2015**, *23*, 2021–2031.
- (32) Weber, W.; Ford, G. Propagation of optical excitations by dipolar interactions in metal nanoparticle chains. *Physical Review B* **2004**, *70*, 125429.
- (33) Koenderink, A. F.; Polman, A. Complex response and polariton-like dispersion splitting in periodic metal nanoparticle chains. *Physical Review B* **2006**, *74*, 033402.
- (34) Park, S. Y.; Stroud, D. Surface-plasmon dispersion relations in chains of metallic nanoparticles: An exact quasistatic calculation. *Physical Review B* **2004**, *69*, 125418.
- (35) Pocock, S. R.; Xiao, X.; Huidobro, P. A.; Giannini, V. Topological plasmonic chain with retardation and radiative effects. *ACS Photonics* **2018**, *5*, 2271–2279.
- (36) Pocock, S. R.; Huidobro, P. A.; Giannini, V. Bulk-edge correspondence and long-range hopping in the topological plasmonic chain. *Nanophotonics* **2019**, *8*, 1337–1347.
- (37) Pan, D.; Yu, R.; Xu, H.; de Abajo, F. J. G. Topologically protected Dirac plasmons in a graphene superlattice. *Nature Communications* **2017**, *8*, 1243.
- (38) Jin, D.; Christensen, T.; Soljačić, M.; Fang, N. X.; Lu, L.; Zhang, X. Infrared topological plasmons in graphene. *Physical Review Letters* **2017**, *118*, 245301.

- (39) Weick, G.; Woollacott, C.; Barnes, W. L.; Hess, O.; Mariani, E. Dirac-like plasmons in honeycomb lattices of metallic nanoparticles. *Physical Review Letters* **2013**, *110*, 106801.
- (40) Han, D.; Lai, Y.; Zi, J.; Zhang, Z.-Q.; Chan, C. T. Dirac spectra and edge states in honeycomb plasmonic lattices. *Physical Review Letters* **2009**, *102*, 123904.
- (41) Wang, L.; Zhang, R.-Y.; Xiao, M.; Han, D.; Chan, C. T.; Wen, W. The existence of topological edge states in honeycomb plasmonic lattices. *New Journal of Physics* **2016**, *18*, 103029.
- (42) Fernique, F.; Weick, G. Plasmons in two-dimensional lattices of near-field coupled nanoparticles. *arXiv preprint arXiv:1905.06727* **2019**,
- (43) Guo, R.; Nečada, M.; Hakala, T. K.; Väkeväinen, A. I.; Törmä, P. Lasing at K Points of a Honeycomb Plasmonic Lattice. *Physical Review Letters* **2019**, *122*, 013901.
- (44) Honari-Latifpour, M.; Yousefi, L. Topological plasmonic edge states in a planar array of metallic nanoparticles. *Nanophotonics* **2019**, *8*, 799–806.
- (45) Maier, S. A.; Kik, P. G.; Atwater, H. A. Optical pulse propagation in metal nanoparticle chain waveguides. *Physical Review B* **2003**, *67*, 205402.
- (46) Moroz, A. Depolarization Field of Spheroidal Particles. *JOSA B* **2009**, *26*, 517–527.
- (47) Yang, H. U.; D’Archangel, J.; Sundheimer, M. L.; Tucker, E.; Boreman, G. D.; Raschke, M. B. Optical dielectric function of silver. *Physical Review B* **2015**, *91*, 235137.
- (48) Zhen, Y.-R.; Fung, K. H.; Chan, C. Collective plasmonic modes in two-dimensional periodic arrays of metal nanoparticles. *Physical Review B* **2008**, *78*, 035419.
- (49) Gorlach, M. A.; Ni, X.; Smirnova, D. A.; Korobkin, D.; Zhirihin, D.; Slobozhanyuk, A. P.; Belov, P. A.; Alù, A.; Khanikaev, A. B. Far-field probing of

- leaky topological states in all-dielectric metasurfaces. *Nature Communications* **2018**, *9*, 909.
- (50) Funston, A. M.; Novo, C.; Davis, T. J.; Mulvaney, P. Plasmon coupling of gold nanorods at short distances and in different geometries. *Nano Letters* **2009**, *9*, 1651–1658.
- (51) Qian, K.; Apigo, D. J.; Prodan, C.; Barlas, Y.; Prodan, E. Topology of the valley-Chern effect. *Physical Review B* **2018**, *98*, 155138.
- (52) Bliokh, K. Y.; Bekshaev, A. Y.; Nori, F. Optical momentum, spin, and angular momentum in dispersive media. *Physical Review Letters* **2017**, *119*, 073901.
- (53) Bliokh, K. Y.; Bekshaev, A. Y.; Nori, F. Optical momentum and angular momentum in complex media: from the Abraham–Minkowski debate to unusual properties of surface plasmon-polaritons. *New Journal of Physics* **2017**, *19*, 123014.
- (54) Baranov, D. G.; Savelev, R. S.; Li, S. V.; Krasnok, A. E.; Alù, A. Modifying magnetic dipole spontaneous emission with nanophotonic structures. *Laser & Photonics Reviews* **2017**, *11*, 1600268.
- (55) Oh, S. S.; Lang, B.; Beggs, D. M.; Huffaker, D. L.; Saba, M.; Hess, O. Chiral Light-matter Interaction in Dielectric Photonic Topological Insulators. Conference on Lasers and Electro-Optics/Pacific Rim. 2018; pp Th4H–5.
- (56) Linton, C. M. Lattice sums for the Helmholtz equation. *SIAM Review* **2010**, *52*, 630–674.